Recurrent Emergence of Boundary Cell Types During Evolution of Floral Bullseye Patterns

Steven Oud [1,2,✉], Maciej M. Żurowski [2], Pjotr L. van der Jagt [1,2], May T. S. Yeo [1,2], Joseph F. Walker [3], Edwige Moyroud [1,2], and Renske M. A. Vroomans [1,2]

[1]The Sainsbury Laboratory, University of Cambridge, Bateman Street, Cambridge CB2 1LR, UK

[2]Department of Genetics, Downing Site, University of Cambridge, Cambridge CB2 3EJ, UK

[3]Department of Biological Sciences, University of Illinois at Chicago, Chicago, IL 60607, USA

Petal patterns contribute to the reproductive success of flowering plants by attracting pollinators and protecting reproductive organs from environmental factors. While some transcription factors (TFs) controlling pigment production and cuticle elaboration have been identified, little is known about the upstream developmental processes that first establish the petal regions where these regulators are active—the pre-patterning phase. Here, we developed a computational model of the evolution and development of petal patterns. We selected for gene regulatory networks (GRNs) that could generate the proximo-distal bullseye pattern of *Hibiscus trionum* petals, which resulted in robust patterning dynamics and a variety of bullseye proportions. We found that the evolution of these bullseye patterns was often accompanied by the spontaneous emergence of a third cell type at the boundary between the proximal and distal regions with a unique gene expression profile. These bullseye boundary cells appeared in the majority of simulations despite not being explicitly selected for, and we validated their presence experimentally in *H. trionum* petals. Although boundary cell types could emerge spontaneously without apparent function, our results indicate they were more often important for pattern formation and more evolutionarily stable when gene expression was noisy. This suggests that this emergent cell type contributes to reproducible bullseye formation by buffering against developmental variability. Altogether, these results illuminate the early steps of petal pattern formation and demonstrate how novel cell types arising spontaneously and repeatedly from selection on other features can help achieve developmental robustness.

Evo-devo | Petal patterning | Gene regulatory networks | Gene expression noise | Boundary establishment | Cell fate

Correspondence: *steven.oud@slcu.cam.ac.uk*

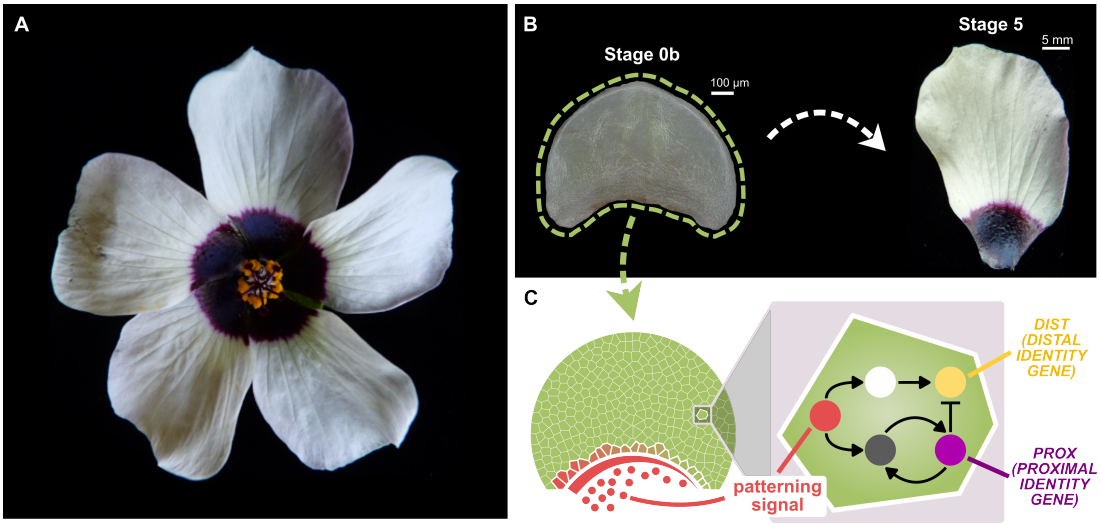

Figure 1. Overview of the *Hibiscus trionum* adaxial petal epidermis and the proposed developmental model of pre-pattern formation in the early-stage petal.
(**A**) The flower of *H. trionum* features a bullseye pattern on its corolla. (**B**) Cell differentiation across the adaxial epidermis of the *H. trionum* petal leads to bullseye formation during petal development. The initially uniform epidermis of the stage 0b petal develops a bilaterally symmetric bicoloured (bullseye) pattern by stage 5.[4] (**C**) A two-dimensional, cell-based model representing the adaxial petal epidermis of Stage 0b in *H. trionum*. Our model assumes that petal patterning is initiated by an external mobile signalling molecule that enters preferentially from one side of the petal due to an asymmetry in the thickness of the petal base.[4] Gene regulation dynamics, governed by a GRN are simulated within each epidermal cell to drive the patterned expression of a *PROXIMAL IDENTITY GENE (PROX)* and a *DISTAL IDENTITY GENE (DIST)*.

Introduction

Flowering plants display a remarkable diversity of colourful and structural patterns on their petal surfaces, including spots, venations, bullseyes, and more complex, composite patterns.[1] These patterns play important roles in determining a flowering plant's reproductive success, influencing both biotic interactions, like pollinator attraction and guidance,[2–4] and abiotic factors, such as protecting reproductive organs from harmful UV radiation or desiccation.[5,6] These roles are not mutually exclusive; in sunflowers, a larger UV-absorbing bullseye is associated with both reduced transpiration rates and increased pollinator attraction.[6] Thus, understanding how these patterns are formed during development and evolve is key to elucidating how morphological adaptation driven by different selection pressures originate and change.

Hibiscus trionum (Malvaceae) has recently been developed as a model species to understand petal pattern development and its evolution.[4,7,8] This herbaceous species produces large flowers with a distinct bullseye pattern, defined by a purple proximal region contrasting with a cream-coloured distal domain (Figure 1A). Cells in these regions also vary in their shape and cuticle texture,[4,7] resulting in a pattern of distinct cell types along the petal proximo-distal axis. The bullseye domains are specified very early in developing *H. trionum* petal primordia, long before cells display the distinct features that characterise the mature petal (Figure 1B).[4,9–11] While progress has been made in identifying the transcription factors (TFs) that directly drive cell differentiation and pigment production in the different regions of the petal,[12–15] much less is known about the upstream regulatory events that actually transform the external signal into a pre-pattern that divides the petal surface into domains, allowing neighbouring cells to follow distinct developmental trajectories.[1,16] One recent hypothesis proposes that the pre-pattern is initiated by an external signal that enters the emerging petal primordium from its base, where it connects to the rest of the floral structure.[4]

Here, we deployed an evolutionary modelling approach[17–20] to develop a computational model of petal pattern evolution and evolve GRNs that can transform a mobile signal into a stable pre-pattern in the *H. trionum* petal primordium. To simulate the developmental dynamics of GRNs, we created a two-dimensional cell-based model of the Stage 0b (as defined in Riglet et al.[4]) adaxial petal epidermis where each cell can differentiate by expressing particular genes (Figure 1C). We then selected gene expression patterns that resembled the distinct proximal and distal bullseye domains observed in *H. trionum* (Figure 1B). To analyse the expression profiles of the various genes from the GRNs that successfully yield bullseye patterns, we developed an analysis pipeline inspired by single-cell RNA sequencing (scRNA-seq) data analysis. This allowed us to investigate the evolution and development of different cell types across the petal surface.

We found that a third cell type evolved at the boundary between the proximal and distal regions in the majority of simulations. This cell type could develop via two distinct but not mutually exclusive mechanisms: (i) by preferentially

expressing a gene only in the boundary region, or (ii) partially overlapping gene expression domains, where the boundary forms in the non-overlapping region. By performing *in silico* targeted mutations, we showed that the specification of the boundary cell type ensures the correct formation of the bullseye pattern. We also demonstrated that such a boundary cell type is indeed present in the *H. trionum* petal, and identified genes that are preferentially expressed at the bullseye boundary region during development in this species. Finally, our data indicate that the evolution of the boundary cell type in our simulations is influenced by the presence of molecular noise in gene transcription and translation; when such noise was absent, the boundary cell type persisted for fewer generations and was often not involved in establishing the proximo-distal pattern. These results suggest that boundary cells play a role in buffering developmental variability during bullseye pattern formation, revealing a novel aspect of petal patterning mechanisms.

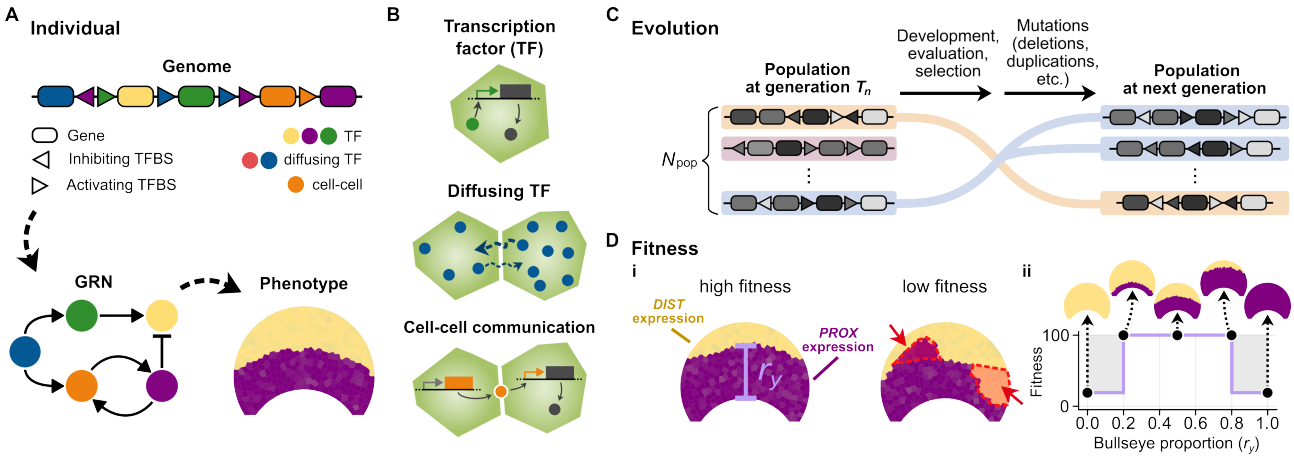

Figure 2. Computational model of petal patterning evolution and development.
(**A**) An individual's genotype is represented by a linear genome comprising genes and transcription factor binding site (TFBS). This genome maps onto a GRN, where genes act as nodes and TFBS serve as edges, either activating or inhibiting interactions. The GRN dynamics are then simulated on the petal tissue to produce a phenotype. (**B**) The proteins of genes can act cell-autonomously as TFs, or as diffusing TFs, or influence transcription in neighbouring cells through cell-to-cell communication. (**C**) Schematic of the evolutionary model used to evolve bullseye patterning mechanisms. In each generation T_n, a population of N_{pop} individuals undergoes development, with phenotypes evaluated and assigned fitness scores. Individuals selected for reproduction pass on their genome to their offspring (the new generation) with a probability of mutations. Mutations include duplication, deletion, innovation, and various changes in gene expression, dissociation rates, and regulatory weights (see Methods). These offspring will undergo development anew, and this cycle is repeated until the final generation T_{gen} is reached. (**D**) Individuals are selected for a bullseye pattern, characterised by mutually exclusive expression domains of *PROX* and *DIST*. (i) Examples of both high-fitness (left) and low-fitness (right) phenotypes. In the low fitness example, unwanted *PROX* and *DIST* expression is marked in red. (ii) The proportion of the bullseye pattern (r_y) is flexible, ranging from 20% and 80% (proximal to total petal height), and can evolve over time.

Results

We constructed a cell-based model of the early-stage *H. trionum* petal adaxial epidermis (Figure 1C) to evolve GRNs of bullseye patterning. A beads-on-a-string-like genome encodes a GRN whose dynamics are simulated in each cell of the petal epidermis (Figure 2A).[21] Genes in the GRN encode proteins that can act cell-autonomously as TFs, diffusing TFs, or cell-cell communication factors (Figure 2B). Development is initialised with all gene expression set to zero, except for the gene coding for the diffusing patterning signal. This signal is constitutively expressed in a subset of cells at the petal base (Figure 1C), representing the entry point of the signal into the petal epidermis. We posit that this signal is distributed asymmetrically, as initial cell area differences across the epidermis always appear first on the thicker side of the petal where it is more thickly attached to the rest of the floral structure.[4] To account for gene expression variability, we introduce noise in the developmental model's molecular processes such as gene transcription and translation (see Methods).

The developmental model determines the phenotype of individuals within an evolving population (Figure 2C). Individuals obtain a high fitness score when their development results in a symmetric bullseye pattern, with the proximal region (centre of the flower bullseye) occupying between 20% and 80% of the petal height, where *PROXIMAL IDENTITY GENE (PROX)* is expressed in the proximal region and *DISTAL IDENTITY GENE (DIST)* in the distal region (Figure 2D). Higher fitness scores result in a higher probability of reproduction, with offspring inheriting their parent's genome with a probability of mutations.

We evolved 35 populations for 30,000 generations in independent evolutionary simulations, all of which successfully evolved GRNs producing robust bullseye patterns (Figure S1). The distribution of maximum fitness achieved in the final generation across simulations is concentrated around a median fitness of approximately 60 out of a theoretical maximum of 100 (Figure 3A.i). This deviation from the maximum primarily results from random fluctuations in gene expression and protein translation due to noise, as all evolved GRNs successfully create a bullseye pattern (Figure S1). We found that over a third of all simulations evolved a bullseye size of approximately 50% of the petal's central height (Figure 3A.ii). This indicates a tendency for simulations to converge toward these proportions, possibly due to the interaction between the patterning signal distribution and the tissue geometry. Nevertheless, a broad range of bullseye dimensions did evolve across simulations (Figure 3A.ii), indicating the existence of GRN architectures that can give rise to variation in bullseye proportions.

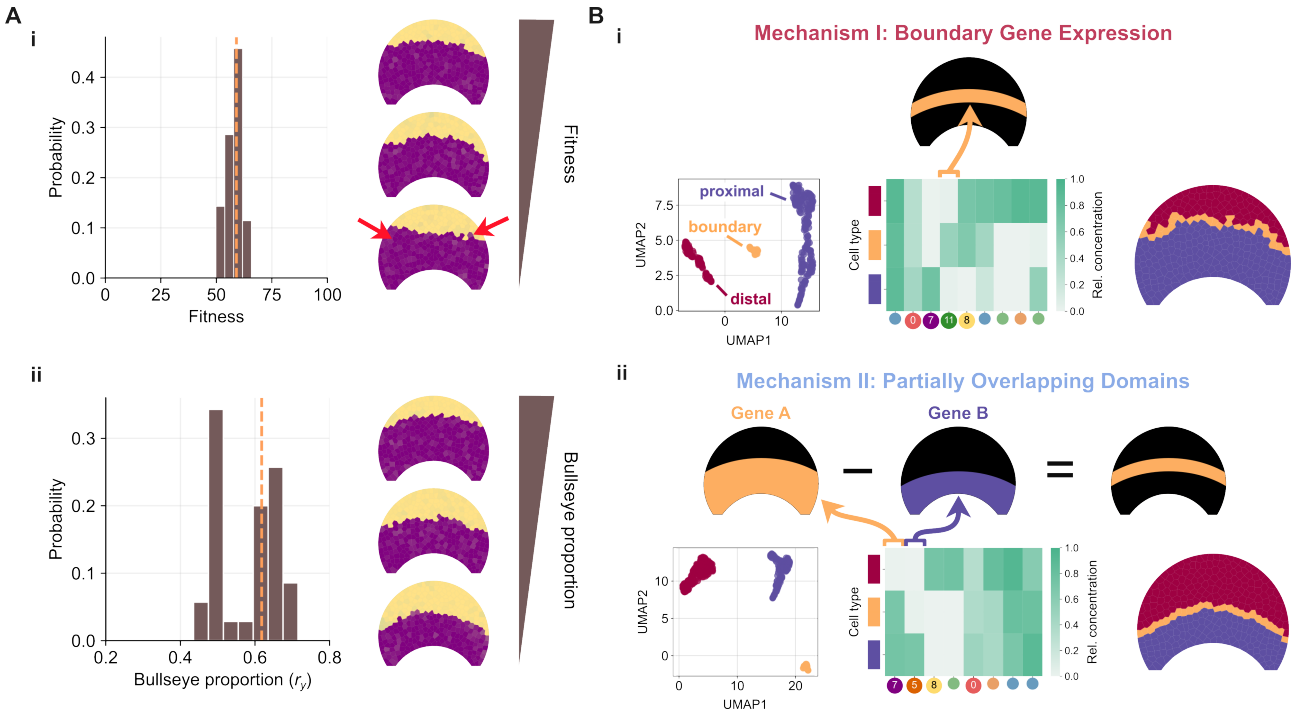

Figure 3. Populations readily evolve bullseye patterning mechanisms and spontaneously evolve boundary cell types. (**A**) Overview of maximum fitness and bullseye proportions in evolved populations. (i) Distribution of maximum fitness achieved by individuals across all simulations. Examples of phenotypes from simulations with varying fitness are shown, with red arrows highlighting an incomplete bullseye pattern in the lowest-fitness simulation. (ii) Overview of bullseye proportions in evolved populations, with example phenotypes from simulations exhibiting different bullseye proportions. Dotted vertical lines indicate medians. (**B**) Two distinct mechanisms drive the spontaneous evolution of boundary cell types. (i) Boundary emergence due to preferential expression of one or more genes in the boundary region (gene 11 in this example). From left to right: UMAP plot showing clustered cells, heatmap of relative protein concentration across the identified cell types, and spatial mapping of these cell types on the petal tissue. Genes not differentially expressed are excluded from the heatmap. (ii) Boundary emergence from overlapping expression domains of uneven lengths. In the example shown, gene 7 (*PROX*) is expressed in the larger bullseye domain (gene A), while gene 5 is expressed in the smaller bullseye domain (gene B).

A third bullseye boundary cell type evolves spontaneously

Next, we wanted to investigate how the evolved gene interactions gave rise to bullseye patterning dynamics. For this, we first assessed the gene expression patterns of all genes involved in forming the bullseye pattern. We performed UMAP dimensionality reduction[22] on the evolved protein states, reducing the 12-dimensional protein space to two dimensions. Next, we performed HDBSCAN clustering[23] on this reduced space to identify different cell types in the petal (Figure S2; see Methods). This analysis was performed for 12 individuals along the ancestral lineage in each simulation. In 26 out of 35 lineages, we found individuals with a third cell type, positioned between the two main regions of the bullseye, in addition to the proximal and distal cell types we selected for. To confirm that the third cluster corresponded to a distinct cell type, we analysed the gene expression profiles of the three identified cell types. This revealed two mechanisms by which the boundary cell type appears: (i) preferential or exclusive expression of certain gene(s) to the boundary region (Figure 3B.i), or (ii) genes displaying overlapping bullseye expression patterns with different proportions (Figure 3B.ii).

Among the 26 simulations in which a boundary cell type evolved, mechanism II was the most common (15/26), followed by cases where both mechanisms co-occurred (8/26; Figure S3A). In contrast, mechanism I rarely evolved on its own (3/26). We hypothesise that mechanism I can emerge neutrally when mechanism II is already present to stabilise the expression of the unique boundary gene in that narrow boundary region (Figure S4B).

Contribution of boundary cell type to bullseye formation

To investigate the role of boundary cell types in bullseye formation, we analysed the pruned GRN (i.e., a GRN in which genes and interactions that have minimal impact on fitness have been removed, see Methods) of a fit individual at generation 30,000 of a representative simulation in which a boundary cell type evolved via mechanism II (Figure 4A). We identified gene 5, a cell-cell communication gene, as a key regulator of boundary cell type formation in this simulation. This gene is expressed in the proximal petal region, following a bullseye pattern one cell smaller in height

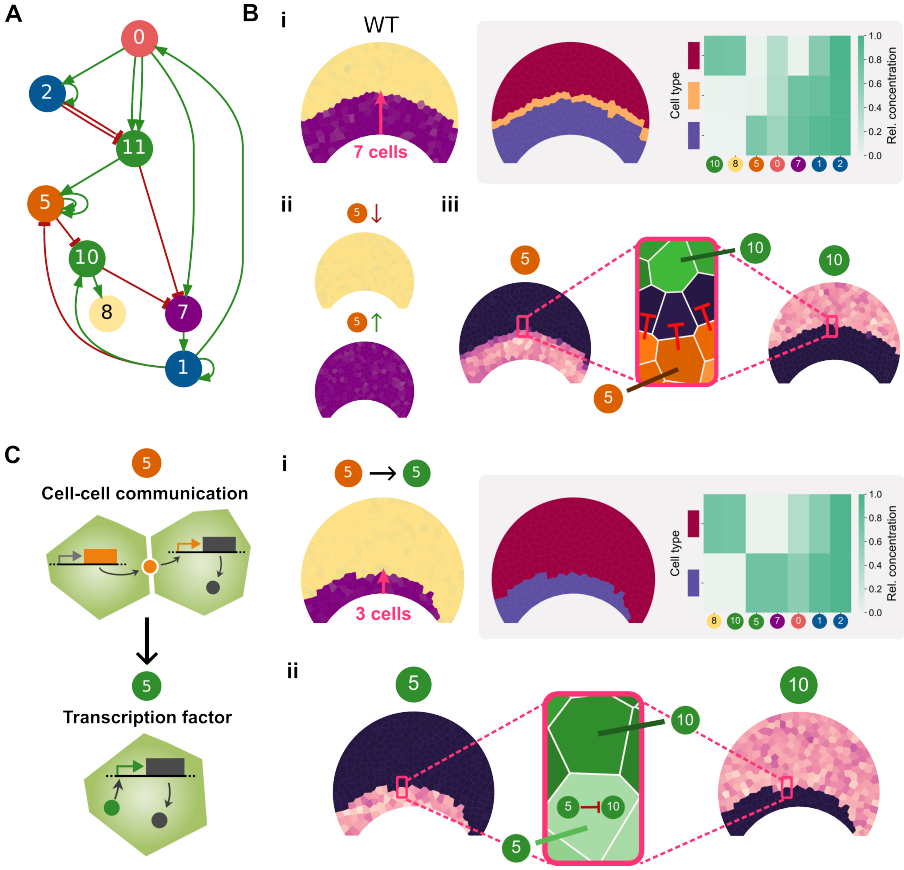

Figure 4. Boundary cell type plays a key role in correct bullseye patterning.
(**A**) Pruned GRN of an individual from a representative simulation at generation 30,000. (**B**) Functional analysis of gene 5 in the GRN. (i) Wild-type phenotype showing normal bullseye pattern formation. (ii) Phenotypic effects of gene 5 knockout and overexpression, both leading to bullseye loss. (iii) Gene 5 restricts gene 10 expression to the distal region via cell-cell signalling, establishing a boundary inhibition zone essential for pattern formation. (**C**) Mutagenesis experiment converting gene 5 from a cell-cell communication gene, which influences neighbouring cells' transcription, to one coding for a transcription factor (TF) acting cell-autonomously, only influencing transcription in cells in which it is expressed. (i) Resulting mutant phenotype showing loss of boundary cell type and bullseye symmetry. (ii) Loss of bullseye boundary inhibition zone due to the inability of gene 5 to regulate gene expression in neighbouring cells.

than the bullseye pattern defined by the expression domain of *PROX* (Figure 4B.i). Disrupting the function of gene 5 by either knockout or overexpressing it constitutively across the petal led to uniform expression of *DIST* and *PROX*, respectively (Figure 4B.ii). In both cases, the bullseye pattern was lost, indicating that gene 5 is required for correct cell differentiation along the proximo-distal petal axis.

Gene 5 is a repressor of gene 10, which is a regulator of distal identity that is preferentially expressed in the distal region and both activates *DIST* and inhibits *PROX* expression (Figure 4A). In turn, gene 5 acts as a regulator of proximal identity, restricting the expression of gene 10 to the distal domain and establishing a boundary inhibition zone through its non-cell-autonomous behaviour (Figure 4B.iii). To further investigate gene 5's contribution to bullseye formation, we modified gene 5 to function as a TF acting cell-autonomously instead of a cell-cell communication gene (Figure 4C). This mutant produced a smaller and asymmetric bullseye pattern, lacking the boundary cell type (Figure 4C.i). Reducing the spatial range of gene 5's regulatory influence by turning it into a TF resulted in a delay in its inhibition of gene 10 and reduced its self-activation range (Figure 4C.ii), explaining the shorter bullseye.

These experiments also show that the bullseye is patterned through a precise timing mechanism. Gene 5 delays the expression of gene 10 both temporally and spatially, ensuring the symmetric development of the bullseye pattern. Without this extended inhibition, boundary cells are lost, and the bullseye becomes misshapen, underscoring the critical role of this cell type in maintaining proper patterning across the petal surface.

Cells at the *H. trionum* bullseye boundary express a unique set of genes during petal development

To test whether the boundary cell type with a unique gene expression profile predicted by our simulations exists in developing petals, we dissected Stage 2 petal primordia (the first stage where the pigmented bullseye become visible)

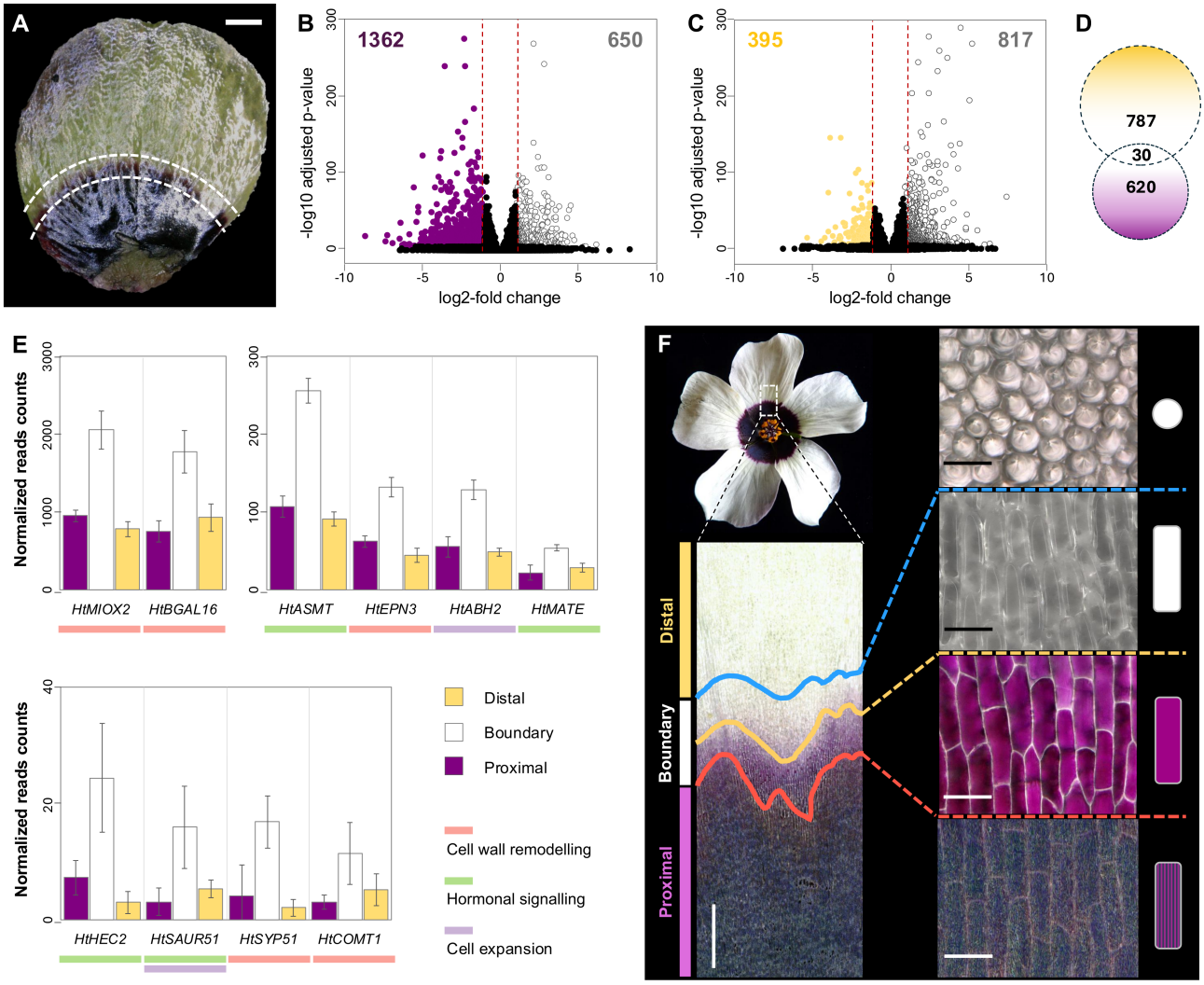

Figure 5. Comparative transcriptomics identifies genes preferentially expressed in the boundary region as bullseye emerges and supports the existence of a distinct boundary cell identity specified at early stages of petal development. (**A**) Dissected wild-type *H. trionum* Stage 2 petal showing the three regions used for RNA extraction and transcriptome analysis: distal (above top dotted line), boundary (between dotted lines), and proximal (below bottom dotted line). Scale bar: 1mm. (**B**, **C**) Volcano plots displaying genes identified in the transcriptome analysis of stage 2 petals. Genes preferentially expressed in the proximal (distal) region (>2x difference compared to boundary) are represented by purple (beige) dots while genes preferentially expressed in the boundary region (>2x difference compared to proximal or distal region) are represented by white dots. Red lines indicate log2-fold thresholds; black dots indicate genes not differentially expressed. (**D**) Venn diagram depicting the genes preferentially expressed in the boundary compared to both proximal or distal regions. The overlap corresponds to genes more expressed in the boundary than in both proximal and distal regions (i.e., boundary genes). (**E**) Expression levels of selected boundary genes involved in cell wall remodelling, hormone signalling, and cell expansion. Transcripts per million (TPM) values are shown; error bars = ±SD with $n = 5$ independent biological replicates. *MIOX2* = *MYO-INOSITOL OXYGENASE 2*, *BGAL16* = Beta-galactosidase16, *ASMT* = *N-ACETYLSEROTONIN O-METHYLTRANSFERASE*, *EPN3* = *EPSIN3*, *ABH2* = abscisic acid 8'-hydroxylase, *MATE* = MATE transporter, *HEC2* = *HECATE2*, *SAUR51* = *SMALL AUXIN UP-REGULATED 51*, *SYP51* = *SYNTAXIN 51*, *COMT1* = *CATECHOL-O-METHYLTRANSFERASE 1*. (**F**) Close-up examination of the petal surface in mature flowers (stage 5) confirms the existence of a visible boundary region where epidermal cell features are distinct from the proximal and distal cells. Boundary cells are flat elongated (tabular) but with a smooth surface. Cells in the lower boundary are anthocyanin-pigmented while cells in the upper boundary are not. Symbols summarise cell types: striped purple rectangle = striated, pigmented, tabular cells; solid purple rectangle = smooth, pigmented, tabular cells; solid white rectangle = smooth, non-pigmented, tabular cells; solid white circle = smooth, non-pigmented, conical cells. Scale bars: central region close-up (left) = 500µm; individual cell types (right) = 50µm.

and used RNA-seq to compare gene expression between the proximal, boundary, and distal petal regions (Figure 5A). We found 650 and 817 genes that were at least expressed twice as much in the boundary region compared to the proximal or distal regions, respectively (Figure 5B,C; Tables S3 and S4). Most of those genes behave as *DIST* (gene

8) from Figure 3B.i and *PROX* (gene 7) from Figure 3B.ii (or gene 7 from Figure 4B.i), respectively. However, 30 of those genes were more expressed in the boundary than anywhere else in the petal (Figure 5D), exhibiting an expression profile similar to the one predicted for gene 11 in Figure 3B.i. This indicates that, although only two epidermal cell types (anthocyanin-pigmented vs. anthocyanin-free) are obviously visible at Stage 2, a third boundary cell type is already present, characterised by unique gene expression patterns as predicted by the model.

Bullseye boundary cells are thought to be specified long before the bullseye emerges, during a pre-patterning phase (Stage S0 to S1).[4] At such an early phase of petal primordia development, epidermal cells have not yet started to produce pigment and have not yet acquired their characteristic shape and texture (pre-differentiation), but the bullseye boundary cells already distinguish themselves as the largest pavement cells across the petal surface.[4] These cells will then differentiate from S1 to S5 to elaborate their typical features, expanding further along the petal axis to become smooth elongated tabular cells (Figure 5F). Among the 30 genes upregulated in the boundary, 7 encode hypothetical or predicted proteins, making their potential roles in bullseye formation difficult to predict. However, over half of the remaining genes (13 out of 23) encode proteins involved in cell wall remodelling, cell expansion and/or hormonal signalling in other species (Figure 5E; Table S5). For example, *MYO-INOSITOL OXYGENASE* catalyses the synthesis of glucuronic acid, a key precursor for cell wall polysaccharides,[24] while Beta-galactosidase16 participates in cell wall biogenesis and remodelling during organ growth.[25–27] *EPSIN3* participates in clathrin-mediated endocytosis, a process vital for wall deposition in apical growing plant cells;[28] SYNTAXINs play crucial roles during exocytosis thus contributing to cytokinesis and the formation and maintenance of cell wall structure, and *CATECHOL-O-METHYLTRANSFERASE* contributes to the synthesis of lignin.[29,30] *ABH2* contributes to ABA metabolism, a hormone known to regulate cell elongation.[31] SAURs are regulators of (polar) cell expansion and mediate auxin-induced acid growth by promoting phosphorylation of plasma membrane H^+-ATPase.[32,33] MATE proteins are also involved in the transport of phytohormones like auxin and abscisic acid.[34] Given the characteristics of the boundary cells, those processes are all likely to contribute to their initial specification and/or their subsequent elaboration during petal development.

Molecular noise increases evolutionary persistence of boundary cell types

To better understand the evolutionary dynamics of the boundary cell types, we measured the number of generations for which they persisted in each simulation (boundary persistence times (BPTs); Figure 6A.i). We find that boundary cell types are most commonly short-lived, persisting for 500 generations or less. However, in several simulations, the boundary cell type persists over long evolutionary times (BPTs longer than 20,000 generations; Figure 6A.ii). To test whether these long-lived boundary types serve a developmental role, we pruned the genomes of individuals from the final generation of simulations with long BPTs, and found that the boundary cell types remained after pruning. Since pruning retains only the genes and interactions essential for bullseye pattern formation, this suggests that in these cases, the mechanisms rely on the boundary cell type to correctly establish proximo-distal differentiation.

Because the boundary in *H. trionum* is specified so early in petal development[4] (pre-patterning phase, Figure 5), we hypothesised that it plays a role in making the patterning process more robust by separating the two main bullseye regions early on. Here, we tested this by performing 35 additional evolutionary simulations without molecular noise, and compared the frequency and distribution of BPTs (Figure 6B; see Methods). Boundary cell types evolved with similar frequencies in both conditions (27/35 simulations without noise vs. 26/35 simulations with noise). However, in most simulations without noise, boundary cells evolved more transiently, appearing and disappearing repeatedly through generations (Figure 6B.i). Additionally, in the absence of noise, we found a notable decrease in the frequency of long BPTs (Figure 6B.ii), suggesting that boundary cell types arise primarily through neutral changes rather than conferring a developmental function or selective advantage. Finally, when pruning the networks that evolved in lineages that exhibited boundary cell types by removing network components with minimal impact on fitness, we found that boundary cell types mostly disappeared in simulations without noise, suggesting that the cell type was a neutral feature. In contrast, a greater proportion of boundary cell types persisted after pruning in simulations with noise (Figure S5). Together, these findings support the idea that boundary cells may help buffer against developmental noise.

We also compared how often each of the two boundary-cell formation mechanisms evolved (Figure 3B) in simulations with and without noise. While mechanism II is most prevalent in the presence of noise (five times more frequent than mechanism I in simulations yielding the boundary cell type; Figure S3A), mechanisms I and II evolved with the same frequency when noise is absent (Figure S3B). Hence, there appears to be no inherent bias towards one mechanism over the other when developmental variability caused by molecular noise is missing. Furthermore, the co-occurrence of both mechanisms was less common than in noisy simulations (Figure S3A,B). These results support our hypothesis that mechanism I by itself is unstable in the presence of molecular noise.

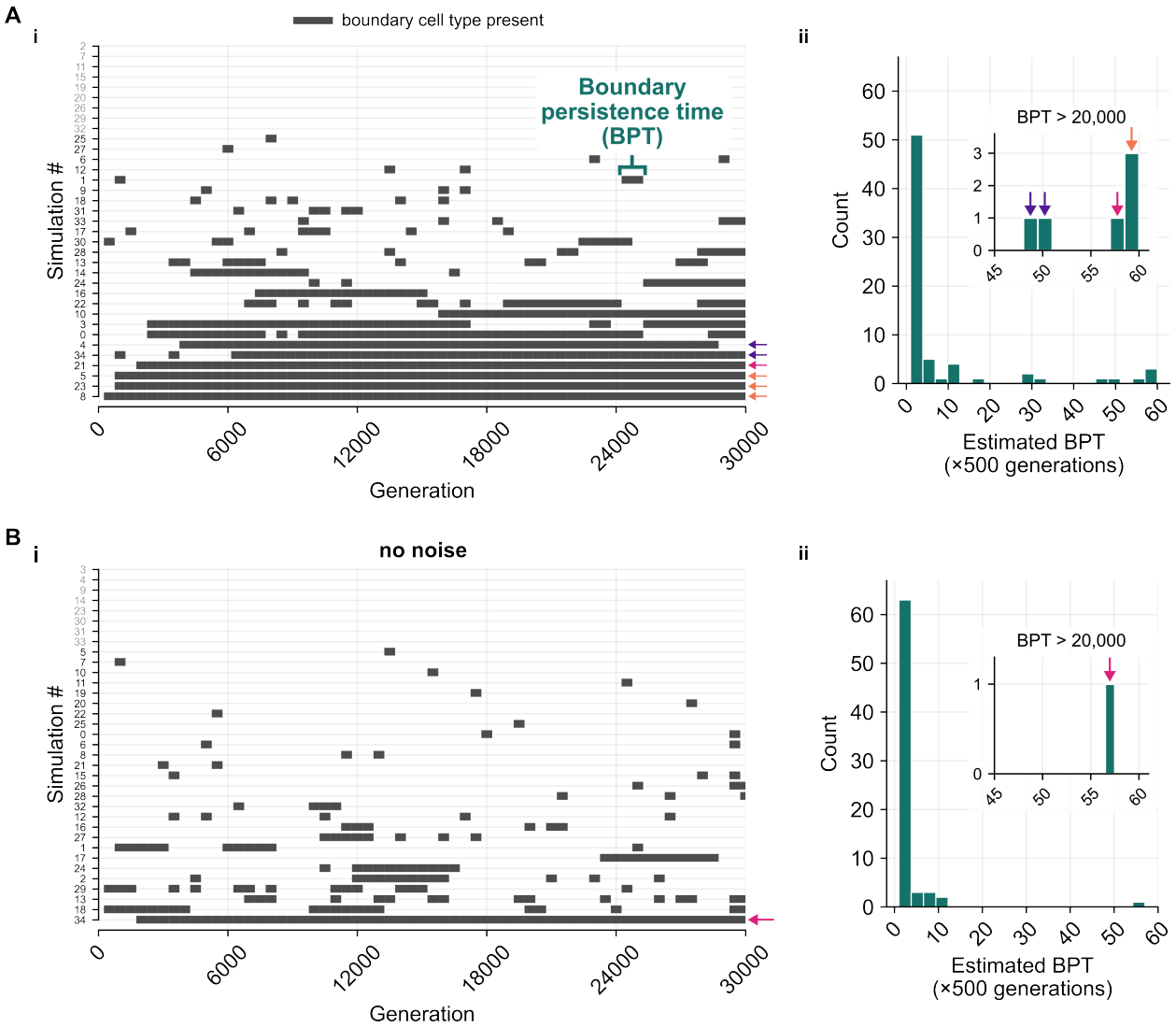

Figure 6. Boundary cell types persist longer during evolution in the presence of molecular noise. (**A**) Evolutionary dynamics of boundary cell types in simulations with molecular noise. (i) Estimated presence of boundary cell types across simulations over 30,000 generations. Boundary cell presence is assessed every 500 generations, introducing a margin of uncertainty of approximately 500 generations. Arrows highlight long BPTs: ∼30,000 generations (orange), ∼28,000 generations (magenta), and ∼25,000 generations (purple). (ii) Distribution of BPTs across simulations. A single simulation may contribute multiple BPTs if boundary cell types reappear throughout evolution or none if no boundary evolved. The inset provides a zoomed-in histogram of long BPTs. (**B**) Evolutionary dynamics of boundary cell types in simulations without molecular noise. (i) Presence of boundary cell types across simulations. (ii) Distribution of BPTs across simulations.

Discussion

In *H. trionum* petals, a bullseye pre-pattern forms early in development, directing downstream processes that generate distinct cell types across the petal surface. Evidence from other species[15,35,36] suggests such pre-patterning events are likely to be widespread across flowering plants, although the underpinning mechanisms accounting for the specification of these boundaries remain to be understood.[37] To start investigating how GRNs establish such early gene expression domains, we developed a cell-based model of the *H. trionum* petal epidermis and evolved GRNs capable of robustly generating bullseye expression patterns. We analysed the successful GRNs with an approach inspired by scRNA-seq data analysis to identify the different cell types present. While our selection criterion specified only two cell types arranged in a bullseye pattern, a third cell type spontaneously emerged at the bullseye boundary in the majority of simulations. We demonstrated that such a boundary cell type exists in the region that separates proximal and distal identity in *H. trionum* petals: pavement cells in this region exhibit a unique combination of structural features (flat tabular shape with a smooth cuticle), and we identified a set of genes preferentially expressed in the bullseye boundary domain. Finally, by comparing simulations with and without molecular noise in the developmental model, we found that boundary cell types are likely not just a neutral side-product of bullseye formation, but instead

could contribute to developmental robustness by buffering against variability in gene expression and other molecular processes. The recent findings from Riglet et al.[4], showing that the *H. trionum* petal is pre-patterned with future bullseye boundary cell differentiating first, is also in agreement with our model and further emphasizes the importance of boundary cells to pattern formation.

Using a transcriptomic approach, we identified 30 genes preferentially expressed in the bullseye boundary region at Stage 2 of petal development in *H. trionum*. These genes fit the predictions of mechanism I and provide experimental support for the existence of a third, distinct boundary cell type, central to bullseye formation. Whether the 30 bullseye boundary genes identified at Stage 2 are involved in the establishment of the bullseye boundary during the pre-patterning phase (Stage 0 to 1, as defined in Riglet et al.[4]) or act later to control the differentiation of the boundary cells (smooth tabular cells seen in Stage 5) remains to be determined. However, the known functions of their homologs in other species (cell wall remodelling, hormone signalling, and cell expansion) are consistent with roles in both the emergence and subsequent differentiation of the bullseye boundary.

Boundary establishment plays an important role during plant development, particularly during morphogenesis, across various regions of the plant.[38–40] Cells in boundary zones are characterised by distinct gene expression profiles and typically exhibit reduced proliferation and growth rates, often contributing to individualisation of emerging primordia or influencing organ shape.[40] The best-characterised boundary genes in plants belong to the NAC (*NAM*, *ATAF1/2*, and *CUC2*) transcription factor family.[41] Loss-of-function mutations of NAC genes cause fusion of adjacent organs[42–47] and leaflets,[47,48] highlighting an important role for boundary genes in maintaining proper organ and leaflet separation during development. Our simulations suggest additional roles for boundary cells in pattern formation. Specifically, we found that boundary cell types may play a role in establishing symmetric bullseye patterns and may buffer pattern formation processes against molecular noise. These results suggest that boundary zones may serve not only structural roles in separating organs during morphogenesis, but also directly contribute to patterning events, playing dynamic roles in ensuring the stability and precision of cell fate specification across a tissue.

Interestingly, a similar boundary pattern was recently reported in the leaves of *Mimulus verbenaceus*, where the patterned expression of three TFs along the proximo-distal leaf axis gave rise to a pigmentation stripe.[49] One of those TFs acts as a proximal identity gene: it is preferentially expressed in the base of emerging leaves and inhibits the activator of pigmentation.[50] Knockout of this gene transformed the leaf pigmentation stripe into a bullseye-like pattern. This suggests that a combination of boundary mechanisms I and II is at play in which the proximal identity gene's smaller bullseye expression domain restricts the activity of the pigmentation activator, otherwise expressed across a larger bullseye region, to the boundary domain, generating the purple leaf stripe. We found that such a combination mechanism is more likely to evolve and be functional in pattern formation when molecular noise is present, suggesting that the boundary pattern in *M. verbenaceus* leaves could initially have emerged to provide developmental stability, later gaining the ability to regulate the expression of pigment biosynthesis genes. Given the shared evolutionary origin of petals and leaves,[51–53] and the comparable proximo-distal organisation observed in both the *M. verbenaceus* leaf pattern and the *H. trionum* petal bullseye, it is possible that boundary cell types are an ancient feature of proximo-distal patterning processes at work in flat lateral organs. Alternatively, as *M. verbenaceus* and *H. trionum* diverged early in angiosperm evolution, around 125 million years ago,[54] they could also have evolved boundary cells independently via replicated evolution, as we demonstrate that boundary cell types can readily and repeatedly evolve in bullseye patterning systems.

Changes in gene regulation and expression have long been considered key drivers of phenotypic novelty.[48,55–58] Novel gene expression patterns could be considered a form of between-level novelty *sensu* Colizzi et al.[59], in which novel mechanisms (e.g., GRNs) evolve to generate a particular phenotype under explicit selection. This type of novelty has been identified recently in the context of developmental systems drift,[20] where regulatory changes alter the underlying patterning mechanisms while maintaining the same phenotypic outcome. These and our simulations highlight that this between-level novelty can also result in novel cell types that either support the development of the trait under selection (a bullseye or stem cell niche pattern), or simply emerge as a neutral by-product. In the case of petal patterning, our results highlight the apparent ease with which evolution can generate boundary cell types in bullseye patterning systems, providing additional support for the idea that the inherent structure and constraints of the developmental system may bias evolution towards specific novel patterns.[60–62]

Finally, our work focused on GRNs of pattern formation in a static tissue, however, Riglet et al.[4] show that morphogenetic processes also influence the proportions of the bullseye pattern, with growth acting as a pattern modifier. The final dimensions of the bullseye therefore result from the combined action of pre-patterning events and regulation of growth in different regions of the petal, with changes to either process potentially affecting bullseye size. Tissue growth may also distort the initial pre-pattern, so additional regulatory feedback between patterning and growth processes may be required to maintain or refine the pattern during petal development.[63] Future work could explore this interplay between pattern formation and morphogenesis by incorporating cell growth and division into the developmental model and evolving patterning mechanisms in a dynamically growing and dividing tissue of cells.

Resource availability

Lead contact. For further information and resources, please contact the lead contact, Steven Oud, at steven.oud@slcu.cam.ac.uk.

Materials availability. This study did not generate new unique reagents.

Data and code availability.

- The coding and genomic sequences of all *H. trionum* genes mentioned in this study can be accessed via the genome of *H. trionum* available on GenBank (https://www.ncbi.nlm.nih.gov/datasets/genome/GCA_030270665.1/) using the HRI_ reference numbers provided in Table S5. The EDWA@ sequences from the reference transcriptome have been published as Supplementary Data 1 in Yeo et al.[8] Transcriptomic data associated with the comparative analysis of gene expression between proximal, boundary, and distal petal regions of *H. trionum* Stage 2 petal (accession numbers SAMN48289654 to SAMN48289683) have been deposited on GenBank SRA (https://www.ncbi.nlm.nih.gov/sra). The algorithms and codes used for RNA-seq data analysis and differential gene expression analysis have been published elsewhere, as indicated in the references provided in the Methods section.
- All original C++ source code and Python analysis scripts used in this work are publicly available at https://gitlab.developers.cam.ac.uk/slcu/teamrv/evo-framework/-/tree/paper-2024-stoch-sims.

Acknowledgements

We acknowledge support from the entire SLCU community including lab support, microscopy, horticulture, and facilities teams. We also thank Enrico Sandro Colizzi and the Sainsbury Laboratory Evolution Journal Club for the helpful discussions and insightful comments on the manuscript.

Funding

This work was supported by grants from the Gatsby Charitable Foundation (G112566) to RMAV; the Gatsby Charitable Foundation (RG92362 and G117782) and the Isaac Newton Trust/Wellcome Trust ISSF (RG89529) to EM.

Author contributions

RMAV and EM conceived and designed the project. SO, PLJ, and RMAV designed the computational model. SO conducted the simulations and analysed simulation data; MMZ developed single-cell inspired analysis pipeline. MTSY and EM performed the experiments; JFW assembled the transcriptomes and performed the differential gene expression analyses between proximal/boundary and distal/boundary; EM analysed the data and identified boundary genes. SO, RMAV, and EM prepared figures and wrote the manuscript, with input from all other authors.

Declaration of interests

The authors declare no competing interests.

Bibliography

1. Fairnie, A. L., Yeo, M. T., Gatti, S., Chan, E., Travaglia, V., Walker, J. F., and Moyroud, E. Eco-evo-devo of petal pigmentation patterning. *Essays in Biochemistry*, 2022.
2. Hirota, S. K., Miki, N., Yasumoto, A. A., and Yahara, T. Uv bullseye contrast of hemerocallis flowers attracts hawkmoths but not swallowtail butterflies. *Ecology and evolution*, 9(1):52–64, 2019.
3. Leonard, A. S. and Papaj, D. R. 'x' marks the spot: The possible benefits of nectar guides to bees and plants. *Functional ecology*, 25(6):1293–1301, 2011.
4. Riglet, L., Zardilis, A., Fairnie, A. L., Yeo, M. T., Jönsson, H., and Moyroud, E. Hibiscus bullseyes reveal mechanisms controlling petal pattern proportions that influence plant-pollinator interactions. *Science Advances*, 10(37):eadp5574, 2024.
5. Koski, M. H. and Ashman, T.-L. Floral pigmentation patterns provide an example of gloger's rule in plants. *Nature Plants*, 1(1): 1–5, 2015.
6. Todesco, M., Bercovich, N., Kim, A., Imerovski, I., Owens, G. L., Ruiz, Ó. D., Holalu, S. V., Madilao, L. L., Jahani, M., Légaré, J.-S., and others, . Genetic basis and dual adaptive role of floral pigmentation in sunflowers. *Elife*, 11:e72072, 2022.
7. Moyroud, E., Airoldi, C. A., Ferria, J., Giorio, C., Steimer, S. S., Rudall, P. J., Prychid, C. J., Halliwell, S., Walker, J. F., Robinson, S., and others, . Cuticle chemistry drives the development of diffraction gratings on the surface of hibiscus trionum petals. *Current Biology*, 32(24):5323–5334, 2022.
8. Yeo, M. T., Fairnie, A. L., Travaglia, V., Walker, J. F., Riglet, L., Zeyrek, S., and Moyroud, E. The genetic basis of replicated bullseye pattern reduction across the hibiscus trionum complex. *New Phytologist*, 2025.

9. Davies, K. M., Albert, N. W., and Schwinn, K. E. From landing lights to mimicry: the molecular regulation of flower colouration and mechanisms for pigmentation patterning. *Functional Plant Biology*, 39(8):619–638, 2012.
10. Kicheva, A. and Briscoe, J. Developmental pattern formation in phases. *Trends in Cell Biology*, 25(10):579–591, 2015.
11. Galipot, P., Damerval, C., and Jabbour, F. The seven ways eukaryotes produce repeated colour motifs on external tissues. *Biological Reviews*, 96(4):1676–1693, 2021.
12. Cooley, A. M., Modliszewski, J. L., Rommel, M. L., and Willis, J. H. Gene duplication in mimulus underlies parallel floral evolution via independent trans-regulatory changes. *Current Biology*, 21(8):700–704, 2011.
13. Martins, T. R., Jiang, P., and Rausher, M. D. How petals change their spots: cis-regulatory re-wiring in clarkia (onagraceae). *New Phytologist*, 216(2):510–518, 2017.
14. Fattorini, R., Khojayori, F. N., Mellers, G., Moyroud, E., Herrero, E., Kellenberger, R. T., Walker, R., Wang, Q., Hill, L., and Glover, B. J. Complex petal spot formation in the beetle daisy (gorteria diffusa) relies on spot-specific accumulation of malonylated anthocyanin regulated by paralogous g d mybsg 6 transcription factors. *New Phytologist*, 2024.
15. Lin, R.-C. and Rausher, M. D. R2r3-myb genes control petal pigmentation patterning in clarkia gracilis ssp. sonomensis (onagraceae). *New Phytologist*, 229(2):1147–1162, 2021.
16. Salvi, E. and Moyroud, E. Building beauty: Understanding how hormone signaling regulates petal patterning and morphogenesis. *The Plant Journal*, 121(6):e70101, 2025.
17. Ten Tusscher, K. H. and Hogeweg, P. Evolution of networks for body plan patterning; interplay of modularity, robustness and evolvability. *PLoS computational biology*, 7(10):e1002208, 2011.
18. Vroomans, R. M., Hogeweg, P., and Ten Tusscher, K. H. In silico evo-devo: reconstructing stages in the evolution of animal segmentation. *EvoDevo*, 7:1–20, 2016.
19. Vroomans, R. M., Hogeweg, P., and Ten Tusscher, K. H. Around the clock: gradient shape and noise impact the evolution of oscillatory segmentation dynamics. *EvoDevo*, 9:1–20, 2018.
20. Jagt, P. L., Oud, S., and Vroomans, R. M. Ubiquitous systems drift in the evolution of development. *bioRxiv*, 2025. doi: $10.1101/2025.04.23.650280$.
21. Crombach, A. and Hogeweg, P. Evolution of evolvability in gene regulatory networks. *PLoS computational biology*, 4(7): e1000112, 2008.
22. McInnes, L., Healy, J., Saul, N., and Grossberger, L. Umap: Uniform manifold approximation and projection. *The Journal of Open Source Software*, 3(29):861, 2018.
23. McInnes, L., Healy, J., and Astels, S. hdbscan: Hierarchical density based clustering. *The Journal of Open Source Software*, 2(11), mar 2017. doi: $10.21105/joss.00205$. URL https://doi.org/10.21105%2Fjoss.00205.
24. Kanter, U., Usadel, B., Guerineau, F., Li, Y., Pauly, M., and Tenhaken, R. The inositol oxygenase gene family of arabidopsis is involved in the biosynthesis of nucleotide sugar precursors for cell-wall matrix polysaccharides. *Planta*, 221:243–254, 2005.
25. Ahn, Y. O., Zheng, M., Bevan, D. R., Esen, A., Shiu, S.-H., Benson, J., Peng, H.-P., Miller, J. T., Cheng, C.-L., Poulton, J. E., and others, . Functional genomic analysis of arabidopsis thaliana glycoside hydrolase family 35. *Phytochemistry*, 68(11): 1510–1520, 2007.
26. Gantulga, D., Ahn, Y. O., Zhou, C., Battogtokh, D., Bevan, D. R., Winkel, B. S., and Esen, A. Comparative characterization of the arabidopsis subfamily a1 β-galactosidases. *Phytochemistry*, 70(17-18):1999–2009, 2009.
27. Chandrasekar, B. and Hoorn, R. A. Beta galactosidases in arabidopsis and tomato–a mini review. *Biochemical Society Transactions*, 44(1):150–158, 2016.
28. Teixeira, R. T., Marchese, D., Duckney, P. J., Dias, F. V., Carapeto, A. P., Louro, M., Silva, M. S., Cordeiro, C., Rodrigues, M. S., and Malhó, R. Functional characterization reveals the importance of arabidopsis eca4 and epsin3 in clathrin mediated endocytosis and wall structure in apical growing cells. *New Phytologist*, 245(3):1056–1071, 2025.
29. Goujon, T., Sibout, R., Pollet, B., Maba, B., Nussaume, L., Bechtold, N., Lu, F., Ralph, J., Mila, I., Barriere, Y., and others, . A new arabidopsis thaliana mutant deficient in the expression of o-methyltransferase impacts lignins and sinapoyl esters. *Plant molecular biology*, 51:973–989, 2003.
30. Weng, J.-K., Akiyama, T., Ralph, J., and Chapple, C. Independent recruitment of an o-methyltransferase for syringyl lignin biosynthesis in selaginella moellendorffii. *The Plant Cell*, 23(7):2708–2724, 2011.
31. Martín, G. and Duque, P. Etiolated hypocotyls: A new system to study the impact of abiotic stress on cell expansion. In *Environmental Responses in Plants: Methods and Protocols*, pages 195–205. Springer, 2022.
32. Mourik, H., Dijk, A. D., Stortenbeker, N., Angenent, G. C., and Bemer, M. Divergent regulation of arabidopsis saur genes: a focus on the saur10-clade. *BMC plant biology*, 17:1–14, 2017.
33. Ren, H. and Gray, W. M. Saur proteins as effectors of hormonal and environmental signals in plant growth. *Molecular plant*, 8 (8):1153–1164, 2015.
34. Upadhyay, N., Kar, D., Deepak Mahajan, B., Nanda, S., Rahiman, R., Panchakshari, N., Bhagavatula, L., and Datta, S. The multitasking abilities of mate transporters in plants. *Journal of experimental botany*, 70(18):4643–4656, 2019.
35. Ding, B., Patterson, E. L., Holalu, S. V., Li, J., Johnson, G. A., Stanley, L. E., Greenlee, A. B., Peng, F., Bradshaw, H. D., Blinov, M. L., Blackman, B. K., and Yuan, Y.-W. Two MYB Proteins in a Self-Organizing Activator-Inhibitor System Produce Spotted Pigmentation Patterns. *Current Biology*, 30(5):802–814.e8, March 2020. ISSN 0960-9822. doi: $10.1016/j.cub.2019.12.067$. URL https://www.sciencedirect.com/science/article/pii/S0960982219317002.
36. Lin, R.-C. and Rausher, M. D. Ancient gene duplications, rather than polyploidization, facilitate diversification of petal pigmentation patterns in clarkia gracilis (onagraceae). *Molecular Biology and Evolution*, 38(12):5528–5538, 2021.
37. Yeo, M. and Moyroud, E. Under the rainbow: novel insights on the mechanisms driving the development and evolution of petal pigmentation. *Current Opinion in Plant Biology, in press*, 2025.
38. Žádníková, P. and Simon, R. How boundaries control plant development. *Current opinion in plant biology*, 17:116–125, 2014.
39. Hepworth, S. R. and Pautot, V. A. Beyond the divide: boundaries for patterning and stem cell regulation in plants. *Frontiers in plant science*, 6:1052, 2015.
40. Wang, Q., Hasson, A., Rossmann, S., and Theres, K. Divide et impera: boundaries shape the plant body and initiate new meristems. *New Phytologist*, 209(2):485–498, 2016.
41. Maugarny, A., Gonçalves, B., Arnaud, N., and Laufs, P. Cuc transcription factors: to the meristem and beyond. In *Plant transcription factors*, pages 229–247. Elsevier, 2016.

42. Souer, E., Houwelingen, A., Kloos, D., Mol, J., and Koes, R. The no apical meristem gene of petunia is required for pattern formation in embryos and flowers and is expressed at meristem and primordia boundaries. *Cell*, 85(2):159–170, 1996.
43. Aida, M., Ishida, T., Fukaki, H., Fujisawa, H., and Tasaka, M. Genes involved in organ separation in arabidopsis: an analysis of the cup-shaped cotyledon mutant. *The plant cell*, 9(6):841–857, 1997.
44. Takada, S., Hibara, K.-i., Ishida, T., and Tasaka, M. The cup-shaped cotyledon1 gene of arabidopsis regulates shoot apical meristem formation. *Development*, 128(7):1127–1135, 2001.
45. Weir, I., Lu, J., Cook, H., Causier, B., Schwarz-Sommer, Z., and Davies, B. Cupuliformis establishes lateral organ boundaries in antirrhinum. 2004.
46. Vroemen, C. W., Mordhorst, A. P., Albrecht, C., Kwaaitaal, M. A., and Vries, S. C. The cup-shaped cotyledon3 gene is required for boundary and shoot meristem formation in arabidopsis. *The Plant Cell*, 15(7):1563–1577, 2003.
47. Cheng, X., Peng, J., Ma, J., Tang, Y., Chen, R., Mysore, K. S., and Wen, J. No apical meristem (mtnam) regulates floral organ identity and lateral organ separation in medicago truncatula. *New Phytologist*, 195(1):71–84, 2012.
48. Berger, Y., Harpaz-Saad, S., Brand, A., Melnik, H., Sirding, N., Alvarez, J. P., Zinder, M., Samach, A., Eshed, Y., and Ori, N. The nac-domain transcription factor goblet specifies leaflet boundaries in compound tomato leaves. 2009.
49. LaFountain, A. M., McMahon, H. E., Reid, N. M., and Yuan, Y.-W. To stripe or not to stripe: the origin of a novel foliar pigmentation pattern in monkeyflowers (mimulus). *New Phytologist*, 237(1):310–322, 2023.
50. LaFountain, A. M., Lin, Q., McMahon, H. E., Min, Y., Ding, B., Gurung, V., Seemann, J. R., and Yuan, Y.-W. A distinct foliar pigmentation pattern formed by activator-repressor gradients upstream of an anthocyanin-activating r2r3-myb. *Cell reports*, 43(7), 2024.
51. Goethe, J. W. Versuch die metamorphose der pflanzen zu erklaren. *Gotha, C. W. Ettinger*, 1790.
52. Coen, E. S. and Meyerowitz, E. M. The war of the whorls: genetic interactions controlling flower development. *Nature*, 353 (6339):31–37, 1991.
53. Goto, K., Kyozuka, J., and Bowman, J. L. Turning floral organs into leaves, leaves into floral organs. *Current Opinion in Genetics & Development*, 11(4):449–456, 2001.
54. Vienne, D. M. Lifemap: exploring the entire tree of life. *PLoS biology*, 14(12):e2001624, 2016.
55. Jacob, F. Evolution and tinkering. *Science*, 196(4295):1161–1166, 1977.
56. King, M.-C. and Wilson, A. C. Evolution at two levels in humans and chimpanzees: Their macromolecules are so alike that regulatory mutations may account for their biological differences. *Science*, 188(4184):107–116, 1975.
57. Hoekstra, H. E. and Coyne, J. A. The locus of evolution: evo devo and the genetics of adaptation. *Evolution*, 61(5):995–1016, 2007.
58. Carroll, S. B., Grenier, J. K., and Weatherbee, S. D. *From DNA to diversity: molecular genetics and the evolution of animal design*. John Wiley & Sons, 2013.
59. Colizzi, E. S., Hogeweg, P., and Vroomans, R. M. Modelling the evolution of novelty: a review. *Essays in Biochemistry*, 66(6): 727–735, 2022.
60. Arthur, W. The effect of development on the direction of evolution: Toward a twenty-first century consensus. *Evolution & Development*, 6(4):282–288, 2004.
61. Salazar-Ciudad, I. and Cano-Fernández, H. Evo-devo beyond development: Generalizing evo-devo to all levels of the phenotypic evolution. *BioEssays*, 45(3):2200205, 2023.
62. Müller, G. B. Evo–devo: extending the evolutionary synthesis. *Nature reviews genetics*, 8(12):943–949, 2007.
63. Salazar-Ciudad, I., Jernvall, J., and Newman, S. A. Mechanisms of pattern formation in development and evolution. 2003.

Methods

Plant material and growing conditions

Wild-type *H. trionum* L. CUBG seeds (voucher CGE00046422) were sourced from the Cambridge University Botanic Gardens, Cambridge, UK. Seeds were imbibed in 90 ℃ H_2O for 10 min, germinated in the dark at 30 ℃ for 48 h before being transferred to Levington High Nutrient M3 compost and grown under glasshouse conditions consisting of a 16 h light/8 h dark photoperiod at 25 ℃ with a minimum radiance of 88 W.m^{-2}.

Tissue collection, RNA extraction and Illumina sequencing for *H. trionum* stage 2 petal transcriptome

Tissue was collected from five individual *H. trionum* CUBG plants to generate five biological replicates: for each biological replicate, Stage 2 (S2) petals (as defined in Moyroud et al.[1]) were harvested and dissected to separate proximal, boundary, and distal regions. RNA extraction, RNA-seq library preparation and Illumina sequencing were performed as described in Yeo et al.[2] Raw reads (accession numbers SAMN48289654 to SAMN48289683) have been deposited on GenBank SRA (https://www.ncbi.nlm.nih.gov/sra).

H. trionum CUBG stage 2 petal transcriptome assembly and differential gene expression analysis

RNA-seq reads were used to assess gene expression and compare transcript abundance between proximal, boundary and distal regions of Stage 2 (S2) petal primordia, as defined in Moyroud et al.[1] Transcriptome assembly and differential gene expression analysis were performed as described in Yeo et al.[2] Genes with log2-fold change < -1 or > 1 and adjusted p-value < 0.05 were considered differentially expressed. Results of the differential gene expression are provided in Table S5.

Flower imaging

To produce Figure 5F, an open flower (Stage 5), as defined in Moyroud et al.[1], was collected in the morning and imaged on black velvet using a Panasonic DMC-FZ38 camera. To produce Figure 5A and Figure 5F, dissected petals from Stage 2 bud and Open flower (Stage 5) were imaged with a Keyence microscope (VHX5000 model) fitted with a VH-Z20R or VH-Z100R lens.

Developmental model

Cell and tissue representation. We represent the stage 0b adaxial petal epidermis of *H. trionum* in two-dimensional space using a vertex-based model. The petal tissue domain Ω is discretised into N_C cells through Voronoi tessellation as follows. Given a set of N_C distinct sites $S = \{\mathbf{s}_1, \mathbf{s}_2, \ldots, \mathbf{s}_{N_C}\}$ where $\mathbf{s}_i \in \Omega$, a cell is defined as the Voronoi cell associated to a site:

$$R(\mathbf{s}_i) = \left\{\mathbf{p} \in \Omega \;\middle|\; \|\mathbf{p} - \mathbf{s}_i\|_2 < \|\mathbf{p} - \mathbf{s}_j\|_2, \mathbf{s}_j \in S, j \neq i\right\}. \tag{1}$$

When Eq. S (1) is applied to all sites, we get the Voronoi diagram

$$\mathcal{V}(S) = \{R(\mathbf{s}_i) \,|\, \mathbf{s}_i \in S\}, \tag{2}$$

which we compute using Fortune's algorithm.[3] The resulting Voronoi diagram can be interpreted as a planar graph $\Gamma = (V, E)$ embedded in two-dimensional Euclidean space. Likewise, each cell $R(\mathbf{s}_i)$ can be thought of as a subgraph $H(\mathbf{s}_i)$ of Γ that contains only the vertices and edges related to site $\mathbf{s}_i$, and whose edges form a convex polygon which resembles the cell boundary. The area of the cell corresponding to site $\mathbf{s}_i$ is then given by the shoelace formula

$$A_i = \frac{1}{2} \sum_{\mu=1}^{n_i} |x_\mu y_{\mu+1} - x_{\mu+1} y_\mu|, \tag{3}$$

where $n_i = |V(H(\mathbf{s}_i))|$ is the number of Voronoi vertices that make up cell i, and x_μ and y_μ are the x and y coordinates of a Voronoi vertex $\mathbf{v}_\mu$ belonging to cell i. Note that Eq. S (3) assumes that the Voronoi vertices are ordered in terms of their occurrence along the cell polygon's perimeter, as well that the vertices loop around, i.e., $\mathbf{v}_{n_i+1} = \mathbf{v}_1$.

To account for slight variation in cell configurations in developing tissues due to noise, we generate N_{morph} distinct petal morphologies by adding a small amount of noise to each site's position. During evolution, individuals are independently assigned a random morphology each generation, such that it will need to evolve mechanisms that are robust against variation in cell configuration.

Cell-cell interactions. Cells can affect the behaviour of neighbouring cells either by exchanging gene products through diffusion or by influencing a neighbouring cell's gene expression directly through cell-cell communication genes. The network through which cell interactions are determined is given by the Delaunay triangulation Γ^*, which corresponds to the dual graph of the Voronoi diagram.In the Delaunay triangulation, the vertices are simply the sites ($V(\Gamma^*) = S$), and two sites $\mathbf{s}_i$ and $\mathbf{s}_j$ are connected by an edge if their Voronoi cells share a common edge:

$$E(\Gamma^*) = \{(\mathbf{s}_i, \mathbf{s}_j) \in S \times S \mid E(H(\mathbf{s}_i)) \cap E(H(\mathbf{s}_j)) \neq \emptyset, i < j\}. \tag{4}$$

That is, two cells are considered to be capable of communication if they share a common edge in the Voronoi diagram. Additionally, the interaction strength between two cells, i.e., the weight of an edge $(\mathbf{s}_i, \mathbf{s}_j) \in E(\Gamma^*)$, is determined by the length of the shared Voronoi edge $e = (\mathbf{v}_s, \mathbf{v}_e)$:

$$w_{i,j} = \|\mathbf{v}_s - \mathbf{v}_e\|_2, \tag{5}$$

which can be thought of as the contact surface area of two cell's cell walls.

Gene expression and regulation. Our developmental model is defined as a system of stochastic differential equations (SDEs) that describes the continuous change in mRNA and protein concentrations of genes in discrete cells in the petal tissue. The dynamics of the system are given by a GRN, which is a directed graph $\mathcal{G} = (V, E)$ that is determined by a genome.[4] A vertex $i \in V(\mathcal{G})$ represents a gene, which has a corresponding gene type $\tau(i) \in \{0, \ldots, 11\}$ that determines the behaviour of the gene's protein. The incoming and outgoing edges of a vertex then correspond to the gene's incoming and outgoing regulatory interactions, respectively.

We model the forward flow from gene to mRNA to protein, with proteins regulating the mRNA transcription rates. In each cell, the regulatory dynamics are governed by the same GRN, whereas mRNA and protein concentrations can vary between cells. Each gene i in cell j has its mRNA concentration modelled by the chemical Langevin equation (CLE)[5]:

$$\begin{aligned} \mathrm{d}G_{i,j} = &[A_{i,j}(\mathbf{P}) - d_i(G_{i,j})]\,\mathrm{d}t \\ &+ \sqrt{|A_{i,j}(\mathbf{P})|}\mathrm{d}B_{j,1} - \sqrt{|d_i(G_{i,j})|}\mathrm{d}B_{j,2}, \end{aligned} \tag{6}$$

where $G_{i,j}$ denotes the mRNA concentration of gene (vertex) i in cell j and B denotes a Wiener process. The promoter activity function $A_{i,j}$ determines the transcription rate based on the transcriptional activity $T_{i,j}$:

$$A_{i,j}(\mathbf{P}) = \alpha_i \frac{T_{i,j}(\mathbf{P})^2}{1 + T_{i,j}(\mathbf{P})^2}, \tag{7}$$

where α_i is the maximum mRNA transcription rate of gene i. The decay function d_i describes the degradation of mRNA:

$$d_i(G_{i,j}) = \lambda_i G_{i,j}, \tag{8}$$

where λ_i is the mRNA decay rate of gene i.

The function $T_{i,j}(\mathbf{P})$ describes the transcriptional activity of gene i by integrating the concentrations of the proteins for which it has one or more TFBSs:

$$T_{i,j}(\mathbf{P}) = \max[0, \sigma_{i,j}(\mathbf{P})], \tag{9}$$

with

$$\sigma_{i,j}(\mathbf{P}) = \underbrace{\sum_{k \in E_{\text{ns}}^-(i)} W_{k,i}\theta_{k,i}(P_{\tau(k),j})}_{\text{non-signalling TFBSs}} + \underbrace{\sum_{k \in E_{\text{s}}^-(i)} W_{k,i}\theta_{k,i}\left(\sum_{m \in \mathcal{N}_j} \frac{w_{j,m}}{A_j} P_{\tau(k),m}\right)}_{\text{signalling TFBSs}}, \tag{10}$$

where

- $P_{l,j}$ denotes the protein concentration of gene type l in cell j.
- $E_{\text{ns}}^-(i)$ and $E_{\text{s}}^-(i)$ are the sets of non-signalling and signalling incoming edges of gene i, respectively.
- $W_{k,i}$ is the edge weight which is -1 when an edge is repressive and 1 when an edge is activating.
- $\theta_{k,i}(x)$ is the Hill function

$$\theta_{k,i}(x) = \frac{x^2}{K_{k,i}^2 + x^2}, \tag{11}$$

  describing the proportion of TFs with gene type $\tau(k)$ bound to the TFBS of a gene i as a function of the concentration of the TF (x here), with $K_{k,i}$ being the dissociation constant.

- $\mathcal{N}_j$ denotes the set of neighbouring cells of cell j, i.e., the vertices to which site $\mathbf{s}_j$ has an edge in the Delaunay triangulation.
- $w_{j,n}$ is the interaction strength between cell j and n determined by their contact surface area (Eq. S (5)).
- A_j is the area of cell j (Eq. S (3)).

We have separate terms in Eq. S (9) for TFBSs with non-signalling and signalling gene types, as regulation by signalling gene types is dependent on the signalling gene's protein concentrations in neighbouring cells. Altogether, Eq. S (9) integrates all inhibiting (negative terms) and activating (positive terms) TFBSs of gene i, which determines the transcriptional activity of gene i. When the effect of inhibiting TFBSs is greater than the effect of activating TFBSs such that their sum is negative, the gene is considered to have no transcriptional activity, i.e., $T_{i,j}(\mathbf{P}) = 0$.

Next, the dynamics of protein concentrations are given by the SDE

$$\begin{aligned} \mathrm{d}P_{l,j} = &\left[R_{l,j}(\mathbf{G}) - E\left(P_{l,j}\right) + \mathcal{D}_l \sum_{m \in \mathcal{N}_j} w_{j,m} \left(\frac{P_{l,m}}{A_m} - \frac{P_{l,j}}{A_j} \right) \right] \mathrm{d}t \\ &+ \sqrt{\left|R_{l,j}(\mathbf{G})\right|} \mathrm{d}B_{j,3} - \sqrt{\left|E\left(P_{l,j}\right)\right|} \mathrm{d}B_{j,4}, \end{aligned} \tag{12}$$

where B again denotes a Wiener process, and

$$R_{l,j}(\mathbf{G}) = \sum_{i \in V(\mathcal{G})} \delta_{\tau(i),l} G_{i,j} \tag{13}$$

represents the translation of all mRNAs that have the same gene type l, i.e., all vertices in the GRN $\mathcal{G}$ for which $\tau(i) = l$. Here, $\delta_{\tau(i),l}$ is the Kronecker delta which enforces the condition $\tau(i) = l$ (i.e., it is 1 if $\tau(i) = l$ and 0 otherwise). Next,

$$E\left(P_{l,j}\right) = \gamma P_{l,j} \tag{14}$$

is protein decay where γ is the global protein decay rate, and $P_{l,j}$ is the concentration of protein l in cell j. Finally, in the diffusion term,

$$\mathcal{D}_l = \begin{cases} D & \text{if } l \text{ is a diffusing gene type} \\ 0 & \text{otherwise} \end{cases}, \tag{15}$$

where D is the protein diffusion base rate. As we have discrete cells whose interactions are described by an undirected graph (the Delaunay triangulation), diffusion is implemented as the discrete Laplace operator. The rate of diffusion is proportional to the contact surface area $w_{j,m}$ of two cells j and m, such that cells with a larger contact surface area exchange proteins at a higher rate. Additionally, the diffusion rates are inversely proportional to the area of the respective cells. Note that protein diffusion remains a deterministic process in this model.

These SDEs are solved using a stochastic equivalent of Ralston's second-order Runge-Kutta method.[6] This method converges to the solution of the Stratonovich of our SDE and has a strong order of 1.[7] The diffusion matrix resulting from protein diffusion in Eq. S (12) is solved using SuperLU,[8] a sparse direct solver that implements supernodal LU factorization.

Deterministic developmental model. Deterministic ordinary differential equations (ODEs) are easily derived from the SDEs. For mRNA, we rewrite Eq. S (6) as an ODE as follows:

$$\frac{\mathrm{d}G_{i,j}}{\mathrm{d}t} = A_{i,j}(\mathbf{P}) - d_i\left(G_{i,j}\right). \tag{16}$$

Similarly, for the proteins (Eq. S (12)):

$$\frac{\mathrm{d}P_{l,j}}{\mathrm{d}t} = R_{l,j}(\mathbf{G}) - E\left(P_{l,j}\right) + \mathcal{D}_l \sum_{m \in \mathcal{N}_j} w_{j,m} \left(\frac{P_{l,m}}{A_m} - \frac{P_{l,j}}{A_j} \right). \tag{17}$$

The resulting system of ODEs is numerically integrated using Ralston's second-order Runge-Kutta method.[6]

Gene types. Genes have a specific type, of which there are 12. Each gene type is identified by a unique number from 0 up to 11 (inclusive), and as a result of gene duplications, there may be several genes with the same gene type. However, there are always only 12 TFs, corresponding to the 12 unique gene types. Individuals in the initial population are initialised with genomes that contain at least one gene of each gene type, and between one and three random TFBSs for each gene. Genes code for TFs that can affect the transcriptional activity of genes if they have a TFBS for the corresponding gene type. These TFs behave in different ways depending on their gene type:

- **Gene types 0, 1, and 2** code for diffusing TFs. These TFs are able to move to neighbouring cells through diffusion.
- **Gene types 3, 4, and 5** code for cell-cell communication TFs that influence the transcription of genes in neighbouring cells instead of the cell where they are expressed. This represents membrane receptor-mediated cell-cell communication, where a ligand (the TF) binds to a receptor protein bound to the membrane of neighbouring cells, which causes a signalling cascade that leads to a change in the target gene's activity in the neighbouring cell.
- **Gene types 6-11** code for immobile TFs that simply affect the transcriptional activity of genes in the cells they are expressed in.

Special identity is assigned to certain genes. Gene type 0 represents the mobile signalling molecule which initiates the patterning of the petal. Gene type 7 represents *PROXIMAL IDENTITY GENE (PROX)*, i.e., a gene that is preferentially expressed in the proximal region of the *H. trionum* petal, and gene type 8 represents *DISTAL IDENTITY GENE (DIST)*, i.e., a gene preferentially expressed in the distal region of the petal.

Signalling condition. Gene type 0 is constitutively expressed in a small subset of cells near the petal base, representing the entry point of the patterning signal into the adaxial petal epidermis:

$$G_{i,j} = \kappa_j S_0 \;\; \forall j \in C_S \text{ if } \tau(i) = 0, \tag{18}$$

where $\kappa_j \in [0,1]$ is the intensity of the signal in cell j, S_0 the baseline constitutive signal expression, and C_S the set of signal-producing cells at the base of the petal. The signal intensity decreases linearly with the x position of the cell:

$$\kappa_j = 1 - 0.016\,(x_j - 10)\,, \tag{19}$$

where x_j is the x position of the centroid (site) of cell j.

Note that the protein translation rate of a gene type is given by the sum of all the mRNA concentrations (Eq. S (12)). Hence, having multiple copies of the signalling gene (gene 0) increases the rate at which the signal enters the system (Eq. S (18)).

Fitness function. Let C denote the set of all cells in the tissue, and $C_P(r_y)$ and $C_D(r_y)$ the subsets of cells belonging to the proximal and distal region of a bullseye with height r_y, respectively. To select for a bullseye pattern, we want the PROX (gene type 7) protein at a certain target concentration $T_P = 200$ in the proximal cells, and the DIST (gene type 8) protein at target concentration T_P in the distal cells. Additionally, we want PROX proteins to have a concentration of 0 in the distal cells, and DIST proteins to have a concentration of 0 in the proximal cells.

Formally, we assign a score for how closely a protein concentration x matches the desired concentration in a cell j for a subset of cells $S \in \{C_P, C_D\}$:

$$s_j(x,S) = \begin{cases} 1 - d(x,T_P) & \text{if } j \in S \\ -d(x,0) & \text{otherwise} \end{cases}, \tag{20}$$

where

$$d(x,T) = \min\left(1, \frac{|T-x|}{T_P}\right) \tag{21}$$

measures the normalised distance between the desired target concentration T and the actual concentration x. The fitness at a discrete time point n is then given by Algorithm 1. That is, an individual's fitness is determined by the correct distribution (i.e., two mutually exclusive domains) of PROX and DIST proteins. An individual's total fitness is the average of Algorithm 1 over a time window at the end of development:

$$\mathcal{F} = \frac{1}{n_{\text{end}} - n_{\text{start}}} \sum_{n=n_{\text{start}}}^{n_{\text{end}}} 100^{F(n,r_y^*)}. \tag{22}$$

Algorithm 1: Bullseye Fitness Function $F(n, r_y)$

Input: Set of proximal cells $C_P(r_y)$ and distal cells $C_D(r_y)$, protein concentrations $\mathbf{P}^{(n)}$
Output: Fitness at time point n for bullseye size r_y, $F(n, r_y)$
$F_P \leftarrow 0$;
$F_D \leftarrow 0$;
for $j \leftarrow 1$ **to** N_{cells} **do**
  $F_P \leftarrow F_P + s_j\left(P_{7,j}^{(n)}, C_P(r_y)\right)$; ▷ `Proximal check`
  $F_D \leftarrow F_D + s_j\left(P_{8,j}^{(n)}, C_D(r_y)\right)$; ▷ `Distal check`
end
return $\frac{1}{2}\left(\frac{F_P}{|C_P(r_y)|} + \frac{F_D}{|C_D(r_y)|}\right)$;

Note that as $F(n, r_y) \in (-\infty, 1]$, the range of $\mathcal{F}$ is $(0, 100]$, i.e., the maximum achievable fitness is 100.

The proximal cells are defined as the cells inside of a horizontal ellipse with height r_y and width $1.02 \cdot r_y$:

$$C_P(r_y) = \left\{ j \in C \,\middle|\, \frac{x_j^2}{(1.02 \cdot r_y)^2} + \frac{y_j^2}{r_y^2} \leq 1 \right\}, \tag{23}$$

and the distal cells are the remaining cells outside the ellipse: $C_D(r_y) = C \setminus C_P(r_y)$. The size of the bullseye pattern (i.e., the sets of proximal and distal cells) is determined by optimising the height r_y of the ellipse at developmental timestep $n = n_{\text{start}}$ such that $F(n, r_y)$ is maximised. Local bounded scalar optimisation is performed using Brent's algorithm[9] to determine the bullseye height:

$$r_y^* = \underset{r_y}{\arg\max}\, F(n_{\text{start}}, r_y). \tag{24}$$

This optimised height r_y^* is then used to evaluate an individual's fitness (Eq. S (22)). Note that we restrict the range of possible values for r_y^* to between 20% and 80% of the petal's height to ensure there is sufficient contrast between the proximal and distal domains, maintaining the appearance of a bullseye pattern.

Genome pruning. By representing the genotype as an explicit genome, the genetic architecture is flexible, where gene and TFBS duplications and deletions can create variation in genome size. Additionally, when a gene is duplicated, its upstream TFBSs are duplicated as well, allowing duplicated genes to change their upstream TFBSs, facilitating sub- and neofunctionalisation of duplicated genes. That is, evolution can tinker with the activity of the duplicated gene without affecting the original gene's functionality. This open-endedness gives the evolutionary model more degrees of freedom, which is suggested to improve evolvability[10] but also generally leads to an increase in the size and complexity of evolved GRNs. To this end, we prune the evolved genomes, removing genes and TFBSs that have little to no effect on an individual's fitness. The GRNs resulting from such pruning are referred to as pruned GRNs.

The pruning process is as follows. We remove each gene and TFBS from the individual's genome one at a time and evaluate the effect of this removal on fitness by repeating development 20 times and averaging the fitness outcomes. If the average fitness change is less than 3% of the individual's fitness, the prune is accepted, and the gene or TFBS is removed from the genome. This process continues until no further deletions meet the 3% threshold.

Evolutionary model

The evolutionary model consists of a population of N_{pop} individuals, each of whom has a linear genome that contains transcription factor (TF)-coding genes as well as transcription factor binding sites (TFBSs) upstream of these genes that determine how their expression is regulated.[4] Individuals are initialised with a genome containing one copy of each gene type, and each gene has on average two TFBSs with random gene types and uniformly random activation or inhibition. The population is evolved for T_{gen} generations. At each generation, individuals undergo development, evaluation, and selection based on their fitness (i.e., how well they produce a bullseye pattern). Individuals are selected to reproduce, sometimes multiple times, and the offspring inherit the parental genome on which random mutations occur.

Selection. Every generation, individuals undergo development in which the genotype is mapped into its corresponding phenotype. Based on how closely the phenotype of an individual $i \in \{1, \ldots, N_{\text{pop}}\}$ resembles a bullseye pattern, they

are assigned a fitness score $\mathcal{F}_i$ (Eq. S (22)). The new population is chosen by taking N_{pop} random individuals from the population, where the probability of an individual being selected is given by

$$P_{\text{select}}(i) = \frac{\mathcal{F}_i}{\sum_{j=1}^{N_{\text{pop}}} \mathcal{F}_j}. \tag{25}$$

That is, the population size remains constant, and the probability of an individual being selected is proportional to their fitness. Each individual is sampled independently, and the same individual can be selected multiple times.

Mutations. After selection, each individual in the selected population can undergo multiple mutations. The following mutations can occur (see Table S1 for a comprehensive list of model parameters including mutation probabilities):

- **Gene duplication**. Each gene has a probability of P_{genedup} to duplicate itself and its TFBSs into a random spot in the genome.
- **Gene deletion**. Each gene has a probability of P_{genedel} to have itself and its TFBSs deleted. Note that at least one copy of each gene type is always maintained over evolution.
- **Gene maximum transcription rate change**. Each gene i has a probability of $P_{\text{genetransc}}$ to change its maximum transcription rate α_i. If the mutation occurs, the new maximum transcription rate becomes $\alpha_i' = \alpha_i + X$, where $X \sim \mathcal{N}(0, \sigma_\alpha)$ is a random variable sampled from a normal distribution with mean 0 and standard deviation σ_α.
- **Gene decay rate change**: Each gene i has a probability of $P_{\text{genedecay}}$ to change its mRNA decay rate λ_i. If the mutation occurs, the new mRNA decay rate becomes $\lambda_i' = \lambda_i + X$ where $X \sim \mathcal{N}(0, \sigma_\lambda)$.
- **TFBS duplication**. Each TFBS has a probability of P_{TFBSDup} to copy itself in front of a random gene.
- **TFBS deletion**. Each TFBS has a probability of P_{TFBSDel} to be deleted.
- **TFBS innovation**. There is a P_{TFBSnew} probability of inserting a TFBS with a random type and weight in front of a random gene.
- **TFBS dissociation constant change**. Each TFBS has a probability of $P_{\text{TFBSChange}}$ to change its dissociation constant $K_{k,i}$. If the mutation occurs, the new dissociation constant becomes $K_{k,i}' = K_{k,i} + X$ where $X \sim \mathcal{N}(0, \sigma_K)$.
- **TFBS type change**. Each TFBS has a probability of P_{TFBStype} to change its gene type, i.e., what the source gene type of the regulatory interaction is.
- **TFBS weight change**. Each TFBS has a probability of P_{TFBSinv} to invert its weight $W_{k,i}$, i.e., go from acting as an activator to an inhibitor and vice versa. If the mutation occurs, the new weight becomes $W_{k,i}' = -W_{k,i}$.

Dimensionality Reduction and Clustering

The Uniform Manifold Approximation and Projection (UMAP) algorithm was used for dimensionality reduction using the UMAP Python library.[11] First, protein concentrations across the tissue were filtered to exclude proteins with low relevance. Specifically, proteins with a total concentration below 10 across the entire tissue or a standard deviation under 5 were removed, as these indicate low overall levels and uniform patterns, respectively. Next, each protein concentration was normalised to its highest expression level across the tissue, giving relative protein concentrations that range between 0 and 1. Finally, UMAP dimensionality reduction was applied to the normalised data. Two distinct UMAP embeddings were used: one for clustering and one for visualisation. The clusterable embedding uses the default UMAP parameters with n_neighbors = 30 and min_dist = 0.0, whereas the visualisation embedding uses n_neighbors = 30 and min_dist = 0.1. The same random state 555 was used for all UMAP embeddings to ensure reproducibility. Subsequent clustering was performed using the HDBSCAN Python library[12] to obtain cell types, which are visualised in a heatmap and ordered based on cell type and gene type using hierarchical clustering. HDBSCAN parameters used were min_samples = 15 and min_cluster_size = 20.

Bibliography

1. Moyroud, E., Airoldi, C. A., Ferria, J., Giorio, C., Steimer, S. S., Rudall, P. J., Prychid, C. J., Halliwell, S., Walker, J. F., Robinson, S., and others, . Cuticle chemistry drives the development of diffraction gratings on the surface of hibiscus trionum petals. *Current Biology*, 32(24):5323–5334, 2022.

2. Yeo, M. T., Fairnie, A. L., Travaglia, V., Walker, J. F., Riglet, L., Zeyrek, S., and Moyroud, E. The genetic basis of replicated bullseye pattern reduction across the hibiscus trionum complex. *New Phytologist*, 2025.
3. Fortune, S. A sweepline algorithm for voronoi diagrams. In *Proceedings of the second annual symposium on Computational geometry*, pages 313–322, 1986.
4. Crombach, A. and Hogeweg, P. Evolution of evolvability in gene regulatory networks. *PLoS computational biology*, 4(7): e1000112, 2008.
5. Gillespie, D. T. The chemical langevin equation. *The Journal of Chemical Physics*, 113(1):297–306, 2000.
6. Ralston, A. Runge-kutta methods with minimum error bounds. *Mathematics of computation*, 16(80):431–437, 1962.
7. Gard, T. *Introduction to Stochastic Differential Equations*. Monographs and textbooks in pure and applied mathematics. M. Dekker, 1988. ISBN 978-0-8247-7776-0.
8. Li, X. S. An overview of superlu: Algorithms, implementation, and user interface. *ACM Transactions on Mathematical Software (TOMS)*, 31(3):302–325, 2005.
9. Brent, R. P. *Algorithms for minimization without derivatives*. Courier Corporation, 2013.
10. Vroomans, R., Ten Tusscher, K. H., Rosa, L., Müller, G. B., and others, . Modeling evolution of developmental gene regulatory networks. *Evolutionary Developmental Biology*, (1):1013, 2021.
11. McInnes, L., Healy, J., Saul, N., and Grossberger, L. Umap: Uniform manifold approximation and projection. *The Journal of Open Source Software*, 3(29):861, 2018.
12. McInnes, L., Healy, J., and Astels, S. hdbscan: Hierarchical density based clustering. *The Journal of Open Source Software*, 2(11), mar 2017. doi: $10.21105/\mathrm{joss}.00205$. URL https://doi.org/10.21105%2Fjoss.00205.

Supplementary Information

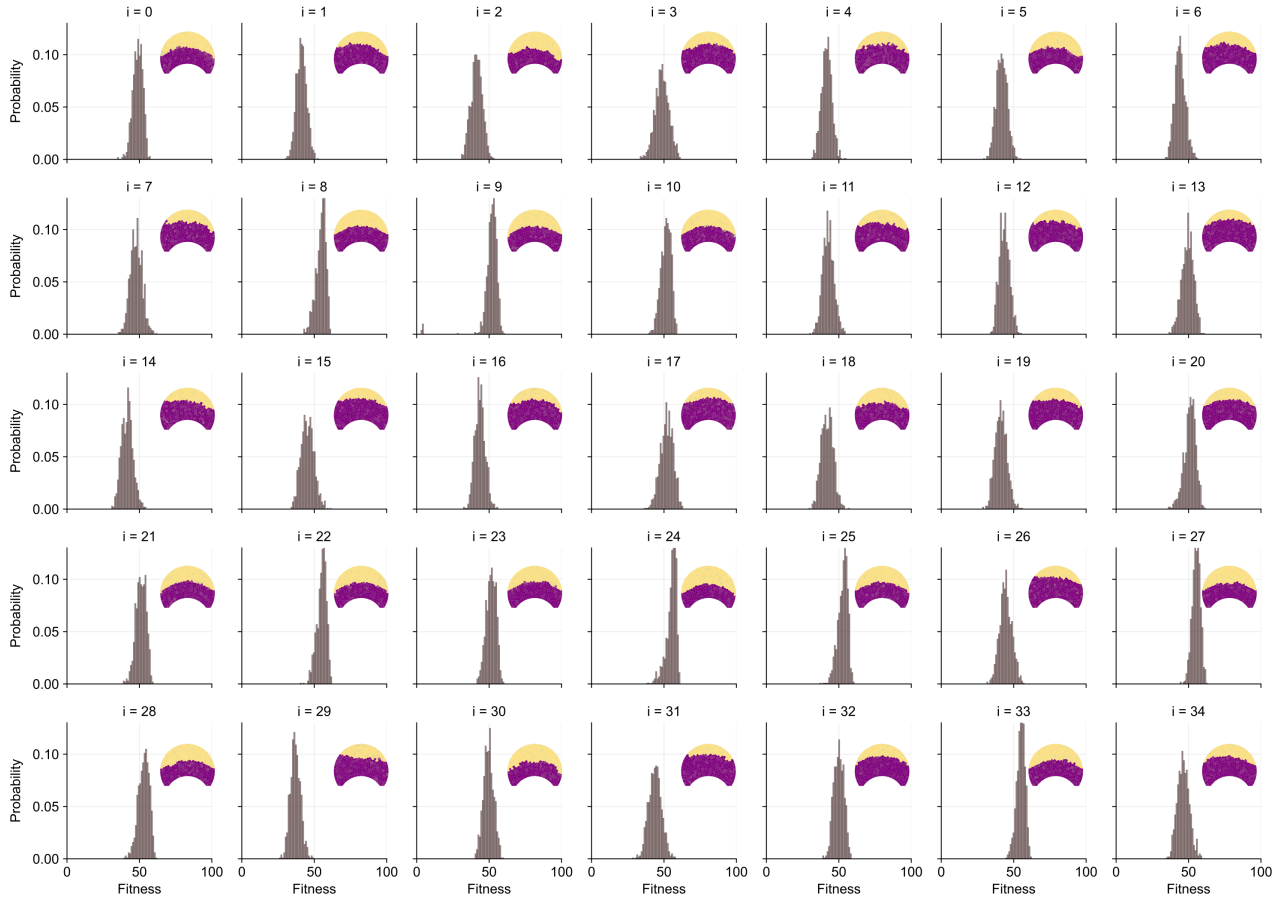

Figure S1. All 35 populations evolved GRNs that robustly generate bullseye patterns. For each simulation, we tested the developmental robustness of the fittest evolved individual by repeating its development 1000 times, each time using a different tissue morphology (see Methods).

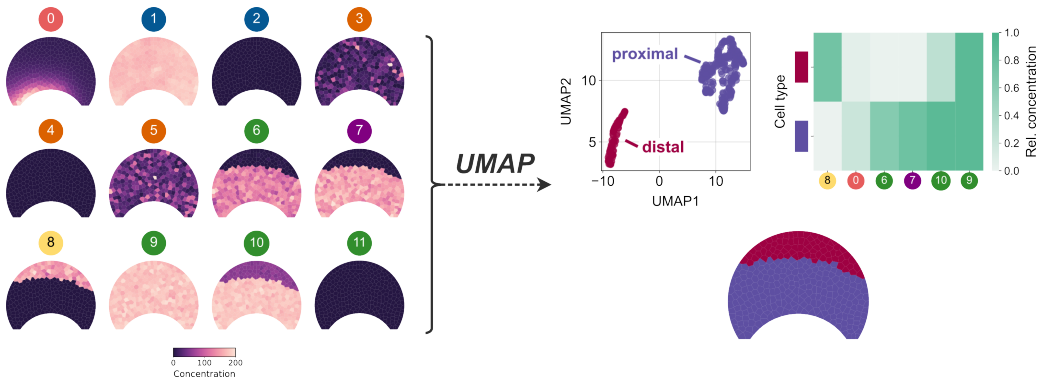

Figure S2. UMAP dimensionality reduction followed by HDBSCAN clustering reveals cell types across petal. UMAP dimensionality reduction was applied to normalized protein concentrations after filtering out low-relevance proteins. HDBSCAN clustering was then performed to identify cell types, which are visualized in a heatmap and across the petal's cells.

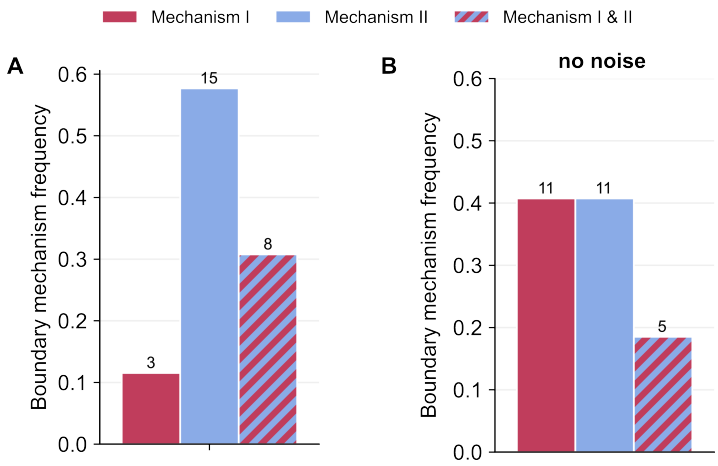

Figure S3. Distribution of boundary mechanisms in the simulations where a boundary cell type appeared in the model with molecular noise (A) and without (B).
The absolute number of occurrences for each mechanism is indicated above each bar.

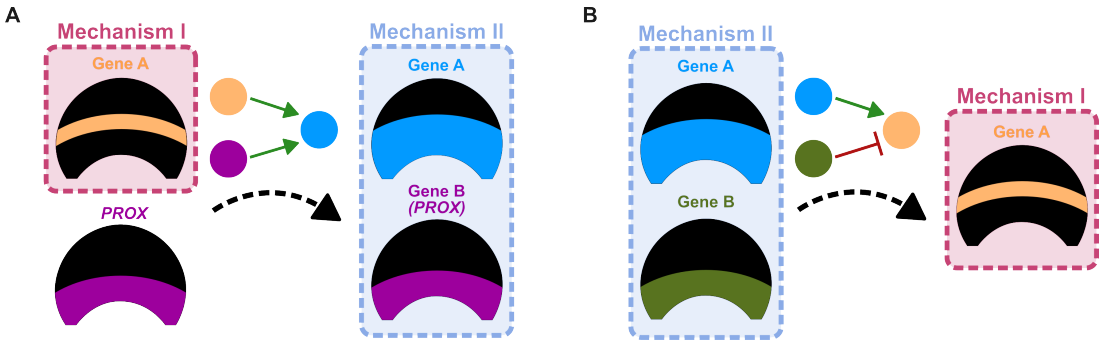

Figure S4. Each boundary mechanism may lead to the emergence of the other.
(**A**) Mechanism I can lead to mechanism II by activation of a gene by both the *PROX* and boundary gene. (**B**) Mechanism II can lead to mechanism I by taking the difference between the two bullseyes through activation of a gene by the larger bullseye and inhibition by the smaller bullseye.

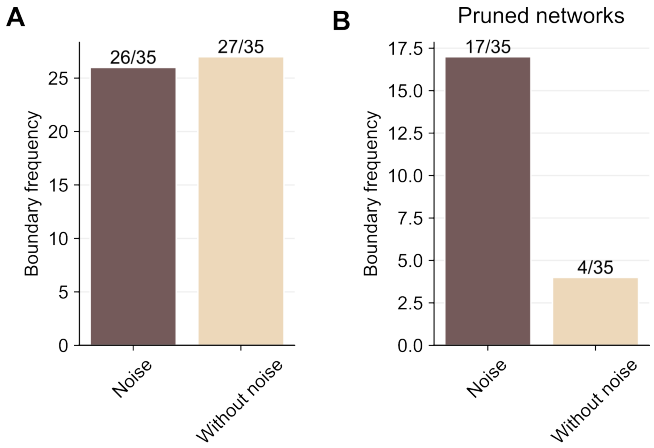

Figure S5. Frequency of evolved boundary cell types across lineages before and after pruning GRNs.
(**A**) Number of simulations that evolved a boundary cell type in their lineage, comparing simulations with and without noise. (**B**) Number of networks that have a boundary cell type after pruning (see Methods), comparing simulations with and without noise.

Supplementary Tables

Table S1. Static parameters for the evolutionary developmental model. Units: M, arbitrary molecular unit; t, arbitrary developmental time unit.

Parameter	Description	Value
Developmental		
N_C	Number of cells in tissue	320
N_{morph}	Number of distinct petal morphologies	1000
D	Protein diffusion base rate	$0.47\,\mu\text{m}\,\text{t}^{-1}$
γ	Protein decay rate	$0.2\,\text{t}^{-1}$
S_0	Baseline constitutive signal expression	$600\,\text{M}\text{t}^{-1}$
T_D	Integration time	$140\,\text{t}$
Δt	Integration step size	$0.2\,\text{t}$
n_{end}	Number of discrete integration steps ($T_D/\Delta t$)	700
n_{start}	Discrete time step at which to start sampling fitness	500
Evolutionary		
N_{pop}	Population size	1000
T_{gen}	Number of generations	30000
α_{init}	Initial maximum transcription rate of a gene	$25\,\text{M}\text{t}^{-1}$
λ_{init}	Initial decay rate of gene mRNA	$0.2\,\text{t}^{-1}$
K_{init}	Initial dissociation constant of a TFBS	$40\,\text{M}$
σ_α	Std. dev. for maximum transcription rate mutations	$5\,\text{M}\text{t}^{-1}$
σ_λ	Std. dev. for mRNA decay rate mutations	$0.01\,\text{t}^{-1}$
σ_K	Std. dev. for dissociation constant mutations	$10\,\text{M}$
P_{genedup}	Probability of gene duplication	0.004 per gene
P_{genedel}	Probability of gene deletion	0.006 per gene
$P_{\text{genetransc}}$	Probability of changing a gene's maximum transcription rate	0.001 per gene
$P_{\text{genedecay}}$	Probability of changing a gene's mRNA decay rate	0.001 per gene
P_{TFBSdup}	Probability of TFBS duplication	0.0011 per TFBS
P_{TFBSdel}	Probability of TFBS deletion	0.0015 per TFBS
P_{TFBSnew}	Probability of inserting a new random TFBS	0.032
$P_{\text{TFBSchange}}$	Probability of changing the dissociation constant of a TFBS	0.004 per TFBS
P_{TFBStype}	Probability of changing the gene type of a TFBS	0.0004 per TFBS
P_{TFBSinv}	Probability of inverting the weight of a TFBS	0.0004 per TFBS

Table S2. Evolvable parameters and their allowed ranges for the developmental model.

Parameter	Description	Value range
α_i	Maximum transcription rate of gene i	$[5, 80]$ Mt^{-1}
λ_i	mRNA decay rate of gene i	$[0.05, 0.9]$ t^{-1}
$K_{k,i}$	Dissociation constant of TFBS k of gene i	$[5, 100]\,\text{M}$
$W_{k,i}$	Regulatory effect (inhibiting or activating) of gene k on gene i	$\{-1, 1\}$

Table S3. Differential gene expression analysis between proximal and boundary regions of Stage 2 *H. trionum* petal primordia.

Table S4. Differential gene expression analysis between distal and boundary regions of Stage 2 *H. trionum* petal primordia.

Table S5. Genes preferentially expressed in the petal bullseye boundary region at Stage 2. Log2 fold Change < -1 or > 1 and $p_{\text{adj}} < 0.05$.